Netrin1 deficiency activates MST1 via UNC5B receptor, promoting dopaminergic apoptosis in Parkinson's disease

Eun Hee Ahn[a], Seong Su Kang[a], Qi Qi[a], Xia Liu[a], and Keqiang Ye[a,1]

[a]Department of Pathology and Laboratory Medicine, Emory University School of Medicine, Atlanta, GA 30322

Edited by Solomon H. Snyder, Johns Hopkins University School of Medicine, Baltimore, MD, and approved June 30, 2020 (received for review March 3, 2020)

The Hippo (MST1/2) pathway plays a critical role in restricting tissue growth in adults and modulating cell proliferation, differentiation, and migration in developing organs. Netrin1, a secreted laminin-related protein, is essential for nervous system development. However, the mechanisms underlying MST1 regulation by the extrinsic signals remain unclear. Here, we demonstrate that Netrin1 reduction in Parkinson's disease (PD) activates MST1, which selectively binds and phosphorylates netrin receptor UNC5B on T428 residue, promoting its apoptotic activation and dopaminergic neuronal loss. Netrin1 deprivation stimulates MST1 activation and interaction with UNC5B, diminishing YAP levels and escalating cell deaths. Knockout of UNC5B abolishes netrin depletion-induced dopaminergic loss, whereas blockade of MST1 phosphorylating UNC5B suppresses neuronal apoptosis. Remarkably, Netrin1 is reduced in PD patient brains, associated with MST1 activation and UNC5B T428 phosphorylation, which is accompanied by YAP reduction and apoptotic activation. Hence, Netrin1 regulates Hippo (MST1) pathway in dopaminergic neuronal loss in PD via UNC5B receptor.

Netrin1 | DCC | UNC5B receptor | Hippo/LATS/YAP signaling | neuronal apoptosis

The core of the Hippo pathway in mammals is a kinase cascade in which the mammalian Ste20-like kinases 1/2 (MST1/2; homologs of *Drosophila* Hippo) phosphorylate and activate large tumor suppressor 1/2 (LATS1/2). The physiological consequence of this kinase cascade is to inhibit the activities of two transcriptional coactivators, Yes-associated protein (YAP) and transcriptional coactivator with PDZ-binding motif (TAZ). When YAP and TAZ are active, they translocate into the nucleus to bind the TEAD transcription factor family and induce expression of a wide range of genes mediating cell proliferation, survival, and migration (1). Physical cues including cell contact and mechanical signals, soluble factors and G protein-coupled receptors (2), and stress signals, etc., activate YAP signaling. Interestingly, several stress signals, such as energy stress, endoplasmic reticulum stress, and hypoxia, can also modulate YAP and TAZ activities (3). MST1/2 have broad functions in addition to regulating core Hippo pathway components of LATS1/2 and YAP/TAZ. Hippo (MST1) pathway is implicated in neuronal cell death. For example, MST1/2 phosphorylate FOXO1 to elicit its nuclear localization and transcription of genes promoting apoptosis in mammalian neurons (4). The apoptotic and functional roles of MST1 in pancreatic β cells appear to be independent of LATS1/2 but rely on PDX1 phosphorylation by MST1 and JNK (5). MST1 phosphorylation is significantly increased in the brain of rats after ICH (intracerebral hemorrhage). Inhibition of MST1 phosphorylation or genetic knockdown of MST1 reduces the activation of P-LATS1 and P-YAP, decreasing neuronal cell death and inflammation in ICH rats. Furthermore, decrease of Mst1 phosphorylation reduces brain edema, blood–brain barrier damage, and neurobehavioral impairment during ICH (6). Previously, we have shown that Akt phosphorylates MST1 on T387 and prevents its proteolytic activation, blocking FOXO3 phosphorylation and nuclear translocation and promoting cell survival (7).

Parkinson's disease (PD) is a neurodegenerative disease that affects movements. PD is characterized by selective loss of dopaminergic neurons in the substantia nigra (SN) pars compacta and dopaminergic innervation in the striatum. Netrins are laminin-related secreted ligands regulating axon guidance and migration through interaction with canonical receptors (8). Netrin1 (NTN1) and its receptors are expressed in dopaminergic neurons and implicated in their axon guidance and growth (9–11). DCC (deletion in colon cancer) and UNC5H (uncoordinated-5 homolog) receptors for NTN1 mediate the signal transduction that occurs in the presence of the ligand NTN1. Interestingly, these molecules act as dependence receptors and are also active in the absence of their ligand. UNC5H or DCC, when expressed in the absence of NTN1, induces cell death, whereas the presence of NTN1 is sufficient for blocking this proapoptotic activity (12–15). DCC is highly expressed in nigral dopamine neurons that are more vulnerable to degeneration (9, 16). Genetic studies show that single nucleotide polymorphisms found in the DCC gene are associated with the susceptibility to develop PD (17, 18). Hence, these findings suggest that NTN1 and its receptors may influence the development and progression of PD. We have previously reported that NTN1 induces interaction of UNC5B receptor (a human homolog for UNC5H2) with the brain-specific GTPase PIKE-L (19). This interaction triggers PI3K/Akt signaling activation, prevents UNC5B's proapoptotic activity, and enhances neuronal survival (20). UNC5B and DCC

Significance

Netrin1 is an important molecule for dopaminergic neuronal survival and axon guidance. The Hippo/MST1/2 pathway plays a critical role in restricting tissue growth in adults and modulating cell proliferation, differentiation, and migration in developing organs as well as in the brain. Here, we demonstrate that Netrin1 is deficient in PD patient's brain that activates Hippo/MST1 kinase, which selectively binds and phosphorylates netrin receptor UNC5B on T428 residue, promoting its apoptotic activation and dopaminergic neuronal loss. Hence, Netrin1 reduction acts as an extrinsic stimulus that triggers Hippo/MST1/YAP pathway activation, leading to dopaminergic neuronal loss in PD pathogenesis.

Author contributions: E.H.A. and K.Y. designed research; E.H.A. performed research; S.S.K., X.L., and K.Y. contributed new reagents/analytic tools; E.H.A., S.S.K., Q.Q., and K.Y. analyzed data; and E.H.A. and K.Y. wrote the paper.

The authors declare no competing interest.

This article is a PNAS Direct Submission.

[1]To whom correspondence may be addressed. Email: kye@emory.edu.

This article contains supporting information online at https://www.pnas.org/lookup/suppl/doi:10.1073/pnas.2004087117/-/DCSupplemental.

First published September 14, 2020.

receptors are cleaved by caspase-3 at position 412 for UNC5B and position 1290 for DCC (12, 14). Mutation of the cleavage sites prevents the proapoptotic activity of these receptors, suggesting that cleavage is a prerequisite for cell death induction by releasing/exposing a proapoptotic domain named addiction dependence domain lying in the intracellular domain of DCC or UNC5H (21).

Although numerous upstream components of the Hippo pathway have been identified, the extracellular ligands and cell surface receptors mediating Hippo pathways remain incompletely understood. In the current study, we report that NTN1 mediates MST1 activation via UNC5B receptor. NTN1 reduction triggers dopaminergic neuronal loss in PD via activating MST1 that subsequently phosphorylates UNC5B on T428 residue, escalating its proteolytic cleavage and apoptosis. Blockade of Mst1 phosphorylation of UNC5B or deletion of UNC5B rescues NTN1 deprivation-elicited dopaminergic loss and motor disorders.

Results

MST1 Selectively Associates with UNC5B but Not with Other Netrin Receptors. We recently reported NTN1 exerts its oncogenic activities via escalating YAP protein levels (22). To explore whether netrin receptors are implicated in associating with Hippo pathway components, we conducted a GST pulldown assay by cotransfecting GST-Mst1 and HA-UNC5B into HEK293 cells. Noticeably, UNC5B FL and apoptotic truncated fragment robustly bound to Mst1 (Fig. 1*A*). Interestingly, only UNC5B but not UNC5A or UNC5C interacted with Mst1 (Fig. 1*B*). On the other hand, although human MST1 and MST2 proteins share 78% identities, MST2 failed to associate with any of the receptors (Fig. 1*C*). Mapping assay showed that the UNC5B intracellular ZU5 domain (amino acids [a.a.] 529 to 631) but not the death domain (a.a. 853 to 945) was implicated in binding to MST1 (*SI Appendix*, Fig. S1*A*). Truncation study with MST1 demonstrated that its N-terminal kinase domain but not the C-terminal regulatory domain was involved in binding to UNC5B receptor (*SI Appendix*, Fig. S1*B*). It is worth noting that DCC receptor was unable to bind to either MST1 or MST2 (*SI Appendix*, Fig. S1 *C* and *D*). To further explore the association between UNC5B receptor and MST1 in vivo, we employed UNC5B flox/flox (f/f) and MST1 f/f mice and infected with control or Cre virus in the brains. Coimmunoprecipitation (CO-IP) and reciprocal CO-IP studies showed that MST1 and UNC5B selectively associated with each other in the control virus-infected brains, and deletion of MST1 or UNC5B abolished the interaction (Fig. 1 *D* and *E*). Thus, MST1 selectively binds to UNC5B receptor in the brain.

MST1 Phosphorylates UNC5B on T428 Residue. MST1 is a stress-activated, proapoptotic kinase which, following caspase cleavage, enters the nucleus and induces chromatin condensation followed by internucleosomal DNA fragmentation (23). UNC5B receptor can be also cleaved by caspase-3 and promotes cell death (21). We wondered whether MST1 phosphorylates UNC5B after association. To test this possibility, we conducted in vitro phosphorylation assay with purified intracellular GST-UNC5B (a.a. 413 to 945) recombinant proteins and GST-MST1 (a.a. 1 to 326) kinase domain or its unphosphorylated T183A mutant in the presence of [γ-^{32}P]-ATP. In addition to the robust autophosphorylation, GST-MST1 also strongly phosphorylated UNC5B intracellular domains, and the phosphorylation activity was reduced by MST1 T183A mutant (Fig. 2*A*). To map the specific phosphorylation residue, we performed the truncation assay and found that the phosphorylation sites were located within a.a. 413 to 631 (Fig. 2*B*). Further mapping and truncation assay demonstrated that T428 was the major phosphorylation residue, as T428A mutation on GST-UNC5B (a.a. 413 to 449) disrupted its phosphorylation by MST1 (Fig. 2*C*). Next, we generated its specific rabbit polyclonal phosphor-T428 antibody (p-T428), which exhibited robust signals on PD patient brain sections via immunohistochemistry (IHC) staining. By contrast, no significant signals were observed on healthy control (*SI Appendix*, Fig. S2*A*). Moreover, we found that the antigen but not control peptide preincubation completely abolished the signals by p-T428 on UNC5B in PD patient SN tissues, validating the

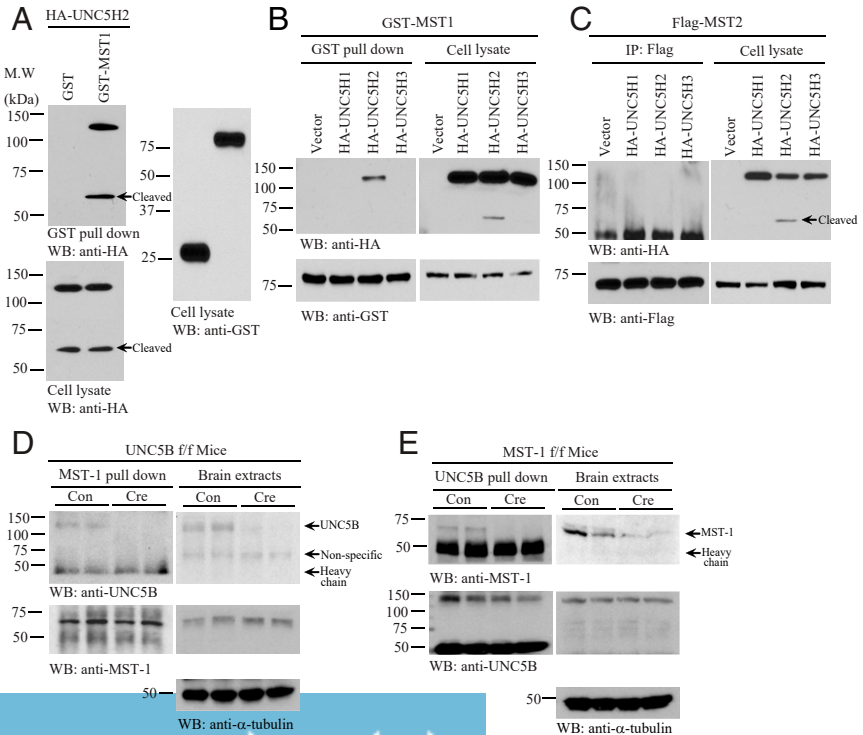

Fig. 1. UNC5B interacts with MST1. (*A*) GST pulldown with HA-UNC5H2 and GST-MST1 cotransfected HEK293 cell lysates. Immunoblots show that MST1 interacted with UNC5B in cotransfected HEK293 cells. (*B*) Mst1 selectively interacts with UNC5H2. GST pulldown from HA-UNC5H1, UNC5BH2, and UNC5H3 and GST-MST1 cotransfected HEK293 cell lysates was detected by immunoblotting. (*C*) Mst2 does not bind to any UNC5 receptors. IP of Flag tag from HA-UNC5H1, UNC5BH2, and UNC5H3 and Flag-MST1 cotransfected HEK293 cell lysates was analyzed by immunoblotting. (*D*) Endogenous MST1 interacts with UNC5B in the brain. CO-IP of MST1 and UNC5B proteins in the control or Cre virus-injected UNC5B f/f mice brain lysates was analyzed by immunoblotting. (*E*) IP of UNC5B from the brain lysates of MST1 f/f mice injected with Cre or control virus was confirmed by immunoblotting. Immunoblots show that MST1 interacted with UNC5B. Three independent studies were conducted in all of the experiments.

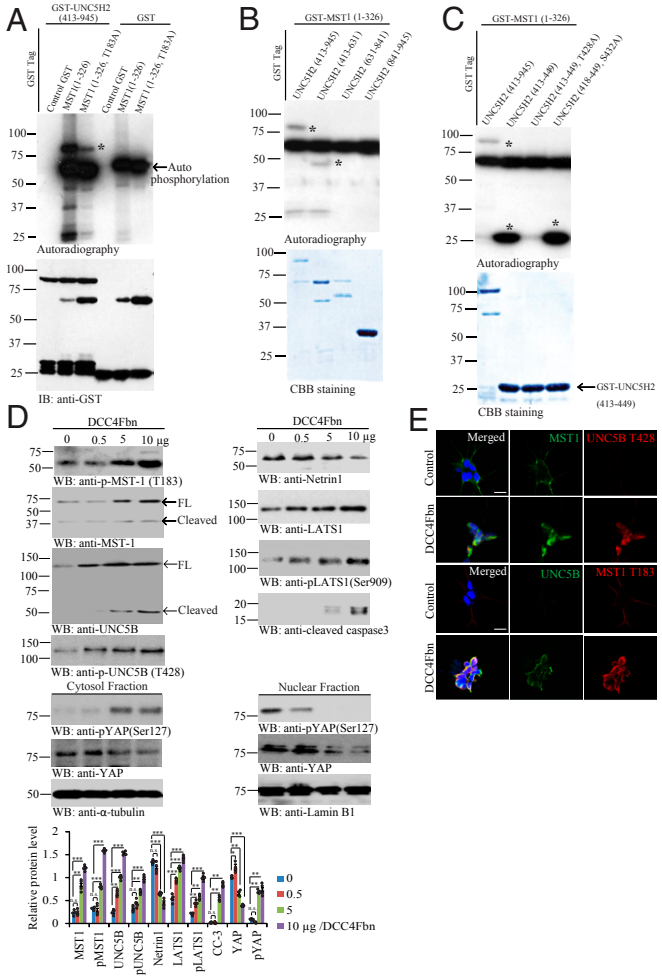

Fig. 2. MST1 phosphorylates UNC5B receptor on Thr-428 residue. (*A*) In vitro autoradiography assay. Purified recombinant GST-UNC5H2 (413 to 945) proteins were incubated with MST1 (1 to 326) or mutated MST1 (1 to 326, T183A) in the presence of [γ-^{32}P]-ATP at 30 °C for 30 min. GST-UNC5H2 (413 to 945) recombinant proteins were strongly phosphorylated by MST1 (1 to 326), and the phosphorylation signals were reduced by MST1 T183A mutant. Both MST1 (1 to 326) and (1 to 326, T183A) fragments were strongly autophosphorylated (*Top*). Control GST was a negative control (*Bottom*). *, represents the autoradiograph specific bands. (*B*) GST-MST (1 to 326) proteins were incubated with UNC5H2 (413 to 945), UNC5H2 (413 to 631), UNC5H2 (631 to 841), and UNC5H2 (841 to 945) in the presence of [γ-^{32}P]-ATP at 30 °C for 30 min. UNC5H2 (413 to 945) and UNC5H2 (413 to 631) domains were selectively phosphorylated (*Top*). *, represents the autoradiograph specific bands. (*C*) GST-MST (1 to 326) proteins were incubated with UNC5H2 (413 to 945), UNC5H2 (413 to 631), UNC5H2 (413 to 449), UNC5H2 (413 to 449, T428A), and UNC5H2 (418 to 449, S432A) in the presence of [γ-^{32}P]-ATP at 30 °C for 30 min. UNC5H2 (413 to 945) domain was determined by autoradiography. Autoradiography showed that UNC5B (T428A) mutant was not phosphorylated; $n = 3$ independent experiments (*Top*). *, represents the autoradiograph specific bands. (*D*) NTN1 deprivation by DCC-4Fbn induces phosphorylation of UNC5B by active MST1. (*Upper Left*) Immunoblot of p-MST1 (T183), MST1, UNC5B, p-UNC5B (T428), (*Upper Right*) NTN1, total LATS1, p-LATS1 (Ser909), cleaved-caspase 3, (*Lower*, cytosol and nuclear fractionation) p-YAP (Ser127), and YAP levels in cell lysates from SH-SY5Y treated with various amount of DCC-4Fbn. DCC-4Fbn elicited p-MST1/p-LATS1/p-YAP signaling activation and YAP degradation and caspase-3 activation; $n = 4$ independent experiments. Error bars represent the mean ± SEM. Statistical significance was determined using a two-way ANOVA followed by post hoc Bonferroni test for multiple group comparison. *$P < 0.05$; **< 0.01; ***$P < 0.001$; n.s., not significant. (*E*) DCC-4Fbn treatment elevates p-MST1 and p-UNNC5B T428 in SH-SY5Y cells. IF costaining representative images used the MST1/p-UNC5B (T428) or UNC5B/p-MST1 (T183) antibodies in NTN1-deprived SH-SY5Y cells. $n = 4$ independent experiments. (Scale bar: 50 μm.)

specificity of p-T428 antibody (*SI Appendix*, Fig. S2*B*), supporting that p-T428 antibody specifically recognizes the p-UNC5B receptor. To investigate whether MST1 phosphorylates UNC5B receptor in intact cells, we utilized dopaminergic cell line SH-SY5Y cells. Treatment with DCC-4Fbn, a recombinant protein from NTN1 binding domain on DCC receptor neutralizing NTN1 (24), dose-dependently triggered MST1 p-T183 escalation, accompanied by prominent MST1 apoptotic cleavage in SH-SY5Y cells. Notably, UNC5B T428 was progressively phosphorylated as the concentrations of DCC-4Fbn gradually increased, which was associated with potent apoptotic fragmentation of UNC5B (Fig. 2 *D*, *Upper Left*). As expected, NTN1 was diminished by DCC-4Fbn in a dose-dependent manner. Interestingly, p-LATS1 S909 and LATS1 total levels were enhanced in a similar way, as was active caspase-3 (Fig. 2 *D*, *Upper Right*). Since YAP phosphorylation dictates its cytoplasmic/nuclear trafficking, accordingly, we prepared the cytosolic and nuclear fractions and found that DCC-4Fbn–stimulated p-YAP S127 activities inversely correlated with total YAP levels in the cytosol, fitting with previous findings that p-YAP S127 triggers its polyubiquitination and degradation. By contrast, in the nuclear fraction, p-YAP S127 activities were dose-dependently reduced, as were total YAP levels, indicating that p-YAP translocates from the nucleus into the cytoplasm (Fig. 2 *D*, *Lower*). Immunofluorescent (IF) costaining on SH-SY5Y cells revealed that MST1 and p-UNC5B T428 were augmented by NTN1 neutralization trap (DCC-4Fbn) as were UNC5B and p-MST1 T183 (Fig. 2*E*), suggesting that NTN1 deprivation activates MST1 that subsequently phosphorylates UNC5B on T428 residue.

NTN1 Deficiency Escalates Mst1 Activation and Binding to UNC5B Receptor. To assess the effect of MST1 kinase activation and UNC5B phosphorylation in their interactions, we cotransfected GST-UNC5B with various Myc-tagged MST1 constructs into HEK293 cells. GST pulldown assay revealed that T183E, a phosphorylation mimetic mutant, strongly interacted with UNC5B as compared to wild-type (WT) MST1, whereas kinase-dead (KD) K59R or unphosphorylated T183A mutant weakly associated with UNC5B (Fig. 3*A*). On the other hand, uncleavable UNC5B D412N mutant displayed the strongest binding activity toward MST1, followed by T428E, a phosphorylation mimetic mutant that revealed stronger binding effect than WT UNC5B. In contrast, T428A, an unphosphorylated UNC5B mutant, failed to associate with MST1 at all (Fig. 3*B*). To assess phosphorylation of UNC5B by MST1 in intact cells, we cotransfected WT or K59R MST1 with HA-UNC5B receptor. UNC5B was immunoprecipitated with anti-HA antibody, and the immunocomplex was monitored with anti-p-Thr antibody. We found that UNC5B was selectively phosphorylated on Threonine by WT but not KD MST1 (Fig. 3*C*). Thus, MST1 binds and phosphorylates UNC5B receptor in the cells.

To examine whether NTN1 regulates MST1 activation, we performed a time course assay with SH-SY5Y cells. NTN1 treatment induced its own up-regulation in SH-SY5Y cells in a time-dependent manner, so was p-Akt, fitting with our previous report (20). Strikingly, p-MST1 T183 was blunted 6 h after NTN1 treatment, and MST1 apoptotic fragmentation was also blocked in a similar manner. As a result, the downstream effector p-LATS S909 and p-YAP S127 signals were temporally repressed by NTN1. Conversely, YAP levels were time-dependently augmented by NTN1, consistent with our previous findings (22) (Fig. 3*D*). Conversely, NTN1 deprivation by DCC-4Fbn showed that NTN1 concentrations were time-dependently reduced. Consequently, p-Akt activities were temporally diminished. Noticeably, p-MST1 T183 was escalated time dependently, coupled with prominent MST1 apoptotic fragmentation. Subsequently, the downstream effectors p-LATS1 S909 and p-YAP S127 were gradually elevated, echoing the upstream p-MST1

activities. Again, YAP's total levels inversely coupled with its p-S127 signals (Fig. 3*E*). To assess the effect of NTN1 stimulation or netrin deprivation in MST1/UNC5B association, we treated SH-SY5Y cells with NTN1 or DCC-4Fbn for 24 h; reciprocal CO-IP assays revealed that netrin deprivation augmented the association between MST1 and UNC5B, while NTN1 treatment antagonized their interactions as compared to phosphate buffered saline (PBS) control. Again, their association tightly correlated with their phosphorylation status on both p-MST1 T183 and p-UNC5B T428 (Fig. 3*F*). Hence, netrin deprivation activates MST1 that binds and phosphorylates UNC5B T428.

Inhibition of UNC5B Phosphorylation by MST1 Blunts Its Proapoptotic Activity. Since both MST1 and UNC5B are implicated in apoptosis, we assessed the role of p-UNC5B T428 by MST1 in its proapoptotic activities separately in HEK293 cells. Terminal deoxynucleotidyltransferase-mediated dUTP nick end labeling (TUNEL) staining showed that overexpression of UNC5B WT or T428E highly induced apoptosis as compared to control, and they both displayed comparable apoptotic effect, whereas T428A revealed significantly decreased apoptotic effect. As expected, MST1 greatly elevated apoptosis, whereas KD K59R mutant exhibited reduced effect. Compared to NTN1 or vehicle control, DCC-4Fbn and mouse monoclonal anti-netrin 2F5 antibody provoked extensive apoptosis (Fig. 4 *A* and *B*). Lactate dehydrogenase (LDH) assay with transfected HEK293 cells displayed a cell death effect similar to UNC5B and MST1. The unphosphorylated UNC5B T428A or KD MST1 revealed attenuated proapoptotic activities as compared to their WT counterparts (*SI Appendix*, Fig. S2*C*). 3-(4,5-dimethylthiazol-2-yl)-2,5-diphenyl tetrazolium bromide (MTT) assay on cell viability indicated an inverse correlation with LDH findings (*SI Appendix*, Fig. S2*D*). To delineate the effect of Mst1 phosphorylation of UNC5B on its proapoptotic activity, we examined various combinations in HEK293 cells. TUNEL assay demonstrated that MST1 phosphorylation of UNC5B enhanced its proapoptotic effect. In the presence of either K59R or unphosphorylated T428A, the apoptosis was evidently mitigated, and the minimal apoptotic effect occurred upon their mixture. On the other hand, cotransfection of T428E and MST1 WT exhibited prominent apoptosis, which was significantly reduced when MST1 WT was replaced by K59R (Fig. 4*C*). These findings were further validated by LDH and MTT assays (*SI Appendix*, Fig. S2 *E* and *F*).

Extensive studies support the cross-talk between prosurvival NTN1 and YAP, which is a transcription coactivator (22, 25, 26). We wondered whether Hippo/MST1 pathway might mediate NTN1 messenger RNA (mRNA) expression. Accordingly, we transfected HEK293 cells with UNC5B WT, T428A, and T428E in the presence or absence of MST1 WT or K59R construct, followed by treatment with vehicle or NTN1. Under control condition, qRT-PCR analysis showed that UNC5B WT or T428E overexpression significantly repressed NTN1 mRNA expression, whereas T428A lost its inhibitory effect. However, MST1 WT or K59R alone had no effect on NTN1 expression. Remarkably, MST1 WT cotransfected with UNC5B WT or T428E further suppressed NTN1 expression, whereas MST1 K59R exhibited reduced suppressive effect. As expected, NTN1 treatment highly augmented its own mRNA expression in all conditions with similar repressive activity by MST1 on UNC5B WT or T428E (Fig. 4*D*). These findings indicate that Mst1 phosphorylating UNC5B escalates its repressive effect on NTN1 mRNA transcription, and NTN1 greatly augments its own transcription. On the other hand, DCC-4Fbn neutralization of NTN1 suppressed its mRNA expression, with MST1 phosphorylation of UNC5B possessing the most robust effect (Fig. 4*E*). Hence, our findings suggest that UNC5B phosphorylation by MST1 elevates its proapoptotic activity, and blockade of its phosphorylation abrogates its proapoptotic effect.

Inhibition of UNC5B Phosphorylation by MST1 Promotes Dopaminergic Neuronal Survival. NTN1 and its receptors are expressed in dopaminergic neurons, modulating axon growth (9–11). To explore the effect of UNC5B and its phosphorylation by MST1 in dopaminergic neuronal loss, we employed UNC5B f/f mice and administrated control or AAV-Cre virus or UNC5B WT, T428A, or T428E virus into the SN region, followed by DCC-4Fbn intraperitoneal (i.p.) injection 1 wk after viral injection. IF costaining with tyrosine hydroxylase (TH), a biomarker for dopaminergic neurons, showed that DCC-4Fbn robustly elevated UNC5B and MST1 and repressed TH signals in the SN (*SI Appendix*, Fig. S3*A*). In alignment with these findings, DCC-4Fbn provoked demonstrable dopaminergic neuronal apoptosis (*SI Appendix*, Fig. S3*B*). Noticeably, endogenous UNC5B receptor in SN was substantially deleted by Cre virus, and UNC5B WT, T428A, and T428E mutants were highly expressed. Overexpression of UNC5B WT or T428E significantly reduced TH fluorescent signals in SN regions (*SI Appendix*, Fig. S4 *A* and *B*). In a month, IHC analysis showed that deletion of UNC5B did not affect TH signals in either SN or striatum. By contrast, overexpression of UNC5B WT or T428E greatly reduced TH activities in both regions. Strikingly, T428A mutant displayed no effect in TH reduction. NTN1 depletion by DCC-4Fbn significantly diminished TH signals under all conditions in both SN and striatum (Fig. 5 *A* and *B* and *SI Appendix*, Fig. S4 *C* and *D*). Motor behavioral assays showed that deletion of UNC5B did not exhibit any abnormal motor dysfunction as compared to control group. It is worth noting that overexpression of UNC5B WT and T428E but not T428A significantly elicited motor deficits in Rotarod, Cylinder, and Grid tests. DCC-4Fbn treatment enhanced the motor disorders in all groups (Fig. 5*C*). Immunoblotting demonstrated that eradication of UNC5B by its Cre virus did not affect TH levels, but eliminated p-MST1 T183 signals in the SN. Subsequently, the downstream effectors p-LATS S909 and p-YAP S127 were attenuated. DCC-4Fbn treatment strongly depleted NTN1 and elicited prominent TH loss, while depletion of UNC5B alleviated TH and NTN1 reduction. Markedly, p-UNC5B T428 was greatly enhanced, which was accompanied by robust UNC5B apoptotic fragmentation. These findings were correlated with evident p-MST1 T183 escalation by DCC-4Fbn; again, p-LATS1 and p-YAP oscillated with the upstream p-MST1 activities. Interestingly, YAP levels were reduced and caspase-3 was activated by DCC-4Fbn, which were attenuated when UNC5B receptor was depleted (Fig. 5*D*).

In alignment with IHC findings, immunoblotting showed that more TH activities and NTN1 occurred in T428A UNC5B infected SN tissues as compared to WT or T428E. Accordingly, p-UNC5B T428's signals and its apoptotic cleavage were evidently reduced. Noticeably, p-MST1 T183 and its apoptotic cleaved active fragment were reduced in T428 UNC5B expressed samples. Consequently, p-LATS S909 and p-YAP S127 signals were mitigated, leading to augmentation of total YAP, which was accompanied with suppression of caspase-3 activation. However, under DCC-4Fbn treatment, active capase-3, p-MST1 T183, and apoptotic MST1 and UNC5B fragmentation were elevated, leading to TH and NTN1 being diminished in the SN, correlating with escalation of p-MST1/p-LATS1/p-YAP signaling (*SI Appendix*, Fig. S5*A*). Quantification of TUNEL-positive cells showed that T428A displayed reduced proapoptotic activity as compared to UNC5B WT and 428E, whereas deletion of UNC5B by Cre virus alone did not trigger any detectable apoptosis. Nonetheless, DCC-4Fbn treatment greatly increased dopaminergic neuronal apoptosis, which was attenuated when UNC5B was depleted. Again, UNC5B T428A revealed reduced proapoptotic activity when compared to UNC5B WT and T428E (*SI Appendix*, Fig. S5*B*). DCC-4Fbn treatment-induced UNC5B receptor up-regulation and

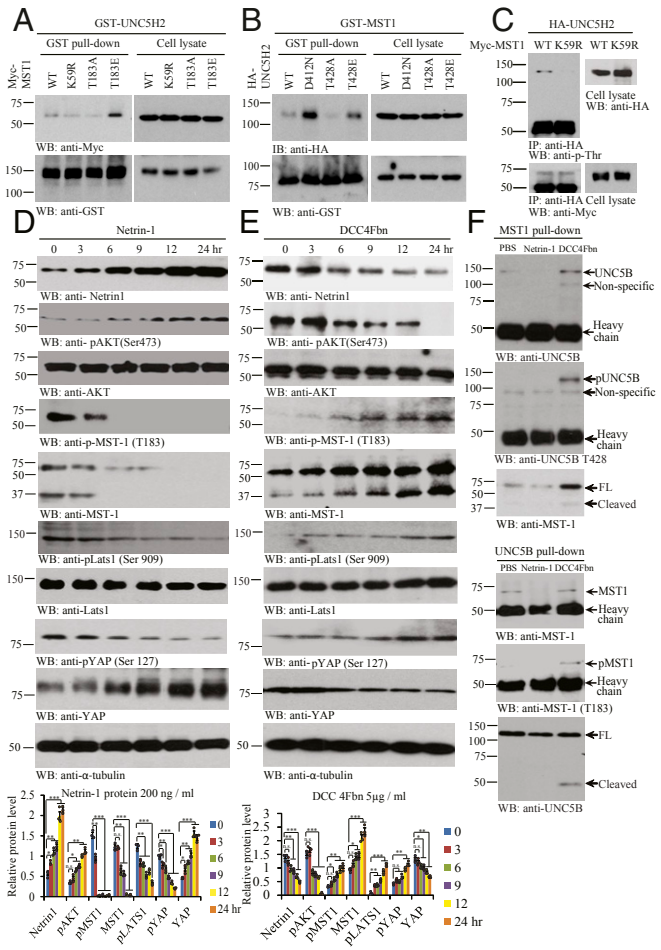

Fig. 3. NTN1 regulates MST1 and UNC5B phosphorylation and association. (*A*) MST1 phosphorylation augments the association between UNC5H2 and MST1. GST pulldown of GST-UNC5H2 in Myc-MST1 WT, Myc-MST1 K59R, Myc-MST1 T183A, or Myc-MST1 T183E cotransfected HEK293 cell was confirmed by immunoblotting. (*B*) Phosphorylated UNC5H2 elevates its interaction with MST1. GST pulldown of GST-MST1 in HA-UNC5H2 WT, HA-UNC5H2 D421N, HA-UNC5H2 T428A, and HA-UNC5H2 T428E cotransfected cells was confirmed by immunoblotting. (*C*) WT but not KD MST1 (K59R) mutant phosphorylates UNC5H2 in intact cells. HA-UNC5H2 immunocomplex from Myc-MST1 WT and Myc-MST1 K59R transfected cell lysates was detected by immunoblotting with anti-p-Thr or anti-Myc. (*D*) NTN1 stimulation inhibits Hippo/MST1 signaling pathway. Protein expression levels (NTN1, pAKT [Ser473], AKT, pMST1 [T183], MST1, pLATS1 [Ser909], Lats1, pYAP [Ser127], and YAP) were analyzed by immunoblotting in the NTN1 protein-treated SH-SY5Y cell lysates. (*E*) NTN1 deprivation activates Hippo/MST1 signaling pathway. Immunoblotting analysis of NTN1, pAKT (Ser473), AKT, pMST1 (T183), MST1, pLATS1 (Ser909), LATS1, pYAP (Ser127), and YAP levels in the DCC-4Fbn–treated SH-SY5Y cell lysates. Error bars represent the mean ± SEM. Statistical significance was determined using a two-way ANOVA followed by post hoc Bonferroni test for multiple group comparison. $*P < 0.05$; $**< 0.01$; $***P < 0.001$; n.s., not significant. (*F*) NTN1 deprivation stimulates UNC5B/MST1 association via reciprocal IP. IPs of MST (upper three panels) and UNC5B (lower three panels) from SH-SY5Y cells treated with vehicle, NTN1, or DCC-4Fbn were analyzed by immunoblotting. Three independent assays were performed in all of the experiments.

TH loss were validated by IF costaining (*SI Appendix*, Fig. S5*C*). Hence, these findings indicate that UNC5B phosphorylation by MST1 is required but not sufficient for its proapoptotic effect in dopaminergic neuronal loss.

KD MST1 K59R Reduces Dopaminergic Neuronal Loss Induced by NTN1 Deprivation. Our data showed that MST1 phosphorylation of UNC5B is indispensable for its proapoptotic activity (Fig. 4). To further explore MST1's role in dopaminergic neuronal loss, we injected control virus or AAV-Cre virus or MST1 WT or KD (K59R) virus in the SN regions in MST1 f/f mice; then DCC-4Fbn was i.p. administered 1 wk after viral injection. IF costaining with antibodies against TH and MST1 revealed that endogenous MST1 in SN was completely depleted by Cre virus, and MST1 WT and K59R mutant were greatly overexpressed. Overexpression of MST1 WT or K59R reduced TH fluorescent signals in SN regions, with the latter revealing reduced activity (*SI Appendix*, Fig. S6 *A* and *B*). In a month, IHC analysis showed that TH activities in the SN region were not altered after MST1 was deleted, whereas overexpression of MST1 WT but not K59R substantially reduced TH signals. DCC-4Fbn treatment potently stimulated TH loss, and TH intensities were significantly higher in MST1 K59R infected dopaminergic neurons as compared to WT (Fig. 6 *A* and *B*). We found a similar pattern for TH intensities in the striatum as well (*SI Appendix*, Fig. S6 *C* and *D*). Motor behavioral tests showed that MST1 WT but not K59R mutant overexpression triggered significant motor disorders as compared to control or Cre group. DCC-4Fbn treatment elicited substantial motor disorders in both control virus and Cre groups and MST1 WT and K59R mutant groups (Fig. 6*C*). Immunoblotting with SN tissues showed that MST1 depletion decreased p-MST1 T183 and p-UNC5B T428 activities and suppressed UNC5B apoptotic cleavage, which were accompanied by reduced p-LATS S909/p-YAP S127. DCC-4Fbn treatment decreased NTN1 and TH levels in the SN, and it also robustly enhanced both MST1 and UNC5B and their apoptotic fragmentation, associated with elevated p-MST1 T183 and p-UNC5B T428, accompanied by prominent apoptotic caspase-3 activation. Consequently, p-LATS S909/p-YAP S127 was escalated upon DCC-4Fbn treatment. All of these events were reduced when MST1 was deleted, resulting in TH escalation (Fig. 6*D*).

Fitting with IHC TH intensities study, immunoblotting also demonstrated that TH levels were higher in MST1 K59R overexpressed samples as compared to WT, as was NTN1. Accordingly, p-MST1 and its apoptotic fragmentation were reduced in K59R overexpressed SN samples, associated with mitigated p-UNC5B T428 and inhibition of UNC5B apoptotic fragmentation. Consequently, p-LATS1 S909/p-YAP S127 signaling was diminished, as was active caspase-3. By contrast, DCC-4Fbn treatment obviously decreased NTN1 and TH levels in MST1 WT infected samples, and it strongly elevated p-MST1 T183 and its apoptotic cleavage, leading to robust p-UNC5B T428 and its apoptotic fragmentation. These events were associated with prominently activated caspase-3 and p-LATS1 S909/p-YAP S127 signaling. Nonetheless, overexpression of K59R Mst1 substantially alleviated these effects, resulting in attenuated caspase-3 activity and higher TH levels (*SI Appendix*, Fig. S7*A*). Quantification of TUNEL activities in TH-positive neurons indicated that overexpression of MST1 WT triggered significantly more dopaminergic neuronal cell death than K59R, whereas deletion of endogenous MST1 did not elicit any demonstrable apoptosis. DCC-4Fbn treatment substantially elicited dopaminergic neuronal apoptosis, but MST1 K59R mutant mitigated dopaminergic neuronal loss induced by DCC-4Fbn (*SI Appendix*, Fig. S7*B*). IF costaining with antibodies against TH and MST1 demonstrated an inverse relationship between TH and MST1 upon DCC-4Fbn stimulation (*SI Appendix*, Fig. S7*C*). Therefore, K59R MST1 mutant blocks NTN1 deprivation-induced dopaminergic neuronal loss and motor dysfunctions.

NTN1 Deficiency in PD Brains Is Associated with Hippo/MST1 Pathway Activation and UNC5B Phosphorylation. Exploring different databases, we found that NTN1 gene expression levels in the SN were significantly decreased in PD patients compared to age-matched health controls, where, in contrast, UNC5B and MST1 were significantly elevated (Fig. 7 *A* and *B*). Immunoblotting showed that NTN1 was evidently reduced in nigral samples from PD

patients compared to the age-matched controls. Remarkably, both UNC5B and MST1 were highly augmented in PD samples with prominent apoptotic fragmentation. As expected, both p-MST1 T183 and p-UNC5B T428 were potently elevated in PD brains. Consequently, the downstream p-LATS S909/p-YAP S127 was increased. Again, the total YAP and TH levels were substantially diminished in PD samples as compared to healthy controls, inversely correlated with active caspase-3 activities (Fig. 7*C*). IF costaining with brain sections confirmed that converse relationship between UNC5B and MST1 up-regulation and TH reduction in PD SN regions (Fig. 7*D*). Accordingly, depletion of Netrin from Netrin f/f mice stimulated p-MST1 T183 and provoked its apoptotic activation, which subsequently phosphorylated UNC5B T428 and elicited its apoptotic fragmentation, leading to caspase-3 activation. Further, p-MST1 elevated p-LATS/p-YAP signalings, resulting in total YAP reduction. By contrast, viral injection of NTN1 into the SN reversed these biochemical events, leading to TH levels escalation (Fig. 7*E*). Hence, our observations support that NTN1 is significantly reduced in PD brains, associated with augmentation of both UNC5B receptor and MST1, which strongly phosphorylates UNC5B T428 and stimulates its apoptotic cleavage, resulting in extensive dopaminergic neuronal loss.

Discussion

In the current study, we show that Hippo/MST1 selectively associates with the dependence receptor UNC5B and mediates its apoptotic activation, when UNC5B cognate ligand NTN1 is deprived. Interestingly, active MST1 strongly phosphorylates UNC5B receptor on the intracellular T428 residue and promotes its apoptotic fragmentation, resulting in extensive dopaminergic cell apoptosis. Consequently, active Hippo/MST1 stimulates the downstream LATS1/YAP effectors phosphorylation and total YAP degradation, which is coupled with prominent caspase-3 activation, culminating in TH-positive dopaminergic neuronal loss in PD patient brains. Mechanistically, we demonstrate that phosphorylation of UNC5B by MST1 plays a critical role in mediating its proapoptotic activities, as UNC5B T428A mutant, which is unphosphorylated by MST1, loses its apoptotic stimulatory effect, although overexpression of phosphorylation mimetic T428E mutant displays apoptotic activity comparable to UNC5B WT. A possible explanation for this discrepancy might be that endogenous MST1/2 readily phosphorylates UNC5B WT into p-UNC5B to trigger its activation, because cotransfection of UNC5B WT with KD MST1 K59R or knockout of endogenous MST1 greatly reduces UNC5B's apoptotic activities (Figs. 4 and 6). Hence, these findings strongly support that MST1 phosphorylation of UNC5B T428 is required for its proapoptotic effect. Employing dopaminergic cell line SH-SY5Y cells, UNC5B f/f mice, and MST1 f/f mice in the presence or absence of NTN1 neutralizing agent DCC-4Fbn, we provide extensive evidence supporting that the cross-talk between MST1 and UNC5B mediates dopaminergic neuronal apoptosis and motor disorders. Moreover, selectively depleting endogenous NTN1 by injecting AAV-Cre virus into the SN region of Netrin f/f mice, we made the similar observations that NTN1 deprivation triggers Hippo/MST1 signaling activation and subsequent UNC5B phosphorylation, which lead to capsase-3 activation and extensive dopaminergic neuronal loss, which is blunted by NTN1 overexpression (Fig. 7*E*). However, we failed to observe Hippo/Mst1 phosphorylation of DCC, indicating that DCC might be involved in PD pathogenesis via different molecular mechanisms, if it is implicated in PD. These findings indicate that NTN1 and UNC5B receptor mediate PD pathogenesis via modulating Hippo/MST1 signaling pathway.

NTN1 has been considered a pro-oncogene due to its oncogenic activity. However, the mechanism by which NTN1 modulates cancer progression is not well understood (27). We have recently reported that NTN1, via its transmembrane receptors, DCC and UNC5B, up-regulates YAP expression, escalating YAP levels in the nucleus and promoting cancer cell proliferation and migration. Surprisingly, MST1/2 is not required for NTN1 to mediate YAP signaling; instead, NTN1 enhances YAP protein stability by stimulating PP1A-induced YAP dephosphorylation in various liver and glioblastoma cancer cells (22). However, in the current study, we demonstrate that NTN1 deprivation or reduction escalates YAP S127 phosphorylation via the canonical Hippo/MST1/LATS pathway and triggers YAP degradation (Figs. 2 and 3). Consistent with these findings, whenever NTN1 is reduced either in the conditional knockout mouse brain or PD patient brains, MST1/LATS/YAP signaling is activated, leading to p-YAP escalation and total YAP decrease and apoptosis augmentation (Fig. 7). In cancer cells, we show that NTN1 increases YAP(total)/actin ratio, but the ratios of p-YAP S127/YAP(total) and p-YAP S397/YAP(total) are actually reduced (22). Nevertheless, NTN1 stimulation temporally inhibits MST1/LATS/YAP pathway in dopaminergic cells, resulting in YAP level accumulation (Fig. 3). Deletion of UNC5B receptor in the brain abolishes MST1 phosphorylation and represses the downstream LATS/YAP pathway, leading to YAP escalation and apoptosis inhibition (Fig. 5). Hence, NTN1 mediates YAP signaling in nervous system that is dependent on UNC5B receptor.

Hippo/MST1 plays an important role in oxidative stress-induced cell death in primary neurons. MST1 mediates oxidative stress-induced neuronal cell death by phosphorylating transcription factor FOXO3 at S207, a site that is conserved in other FOXO family members (4). In addition, c-Abl phosphorylates MST1 at Y433 and increases its kinase activity, mediating oxidative stress-induced neuronal cell death (28). MST1 phosphorylation of FOXO1 at S212, corresponding to S207 in FOXO3, disrupts the association of FOXO1 with 14-3-3. Accordingly, MST1 triggers nuclear translocation of FOXO1 in primary cerebellar granule neurons that are deprived of neuronal activity, triggering neuronal cell death (29). Further, MST1 also mediates stroke-induced microglial activation by directly phosphorylating IκBα at S32 and S36, and Src kinase functions upstream of MST1-IκB signaling during microglial activation. Specific deletion of MST1 in microglia mitigates stroke-induced brain injury. It has been proposed that Src-MST1-IκB signaling plays a critical role in stroke-induced microglial activation (30). Moreover, neuroinflammation up-regulates MST1 that promotes neuronal cell death via JNK and caspase-3 signaling (31, 32). MST1 consists of an N-terminal catalytic domain in the Ste20 class, followed by a noncatalytic tail comprising an autoinhibitory domain and a coiled-coil domain that mediates dimerization (33). It has been suggested that, physiologically, MST1 exists as an autoinhibitory homodimer that is activated after posttranslational modification such as phosphorylation and/or cleavage. MST1 kinase activation requires phosphorylation on T183 and proteolytic degradation by caspases (34). Although caspase-mediated cleavage removes the C-terminal regulatory domain, which is associated with an increase in MST1 activity, there is evidence that caspase-mediated cleavage alone cannot activate Mst1, and both phosphorylation and proteolysis are necessary to fully activate this enzyme (35–37). The Hippo kinase cascade can be initiated by TAO kinases (TAOK1/2/3), which phosphorylate the activation loop of MST1/2 (T183 for MST1 and T180 for MST2) and thereby lead to MST1/2 activation (38, 39). Moreover, the activation loop phosphorylation can be achieved by MST1/2 autophosphorylation (40). Thus, presumably, MST1/2 activation is initiated by dimerization and does not necessarily require upstream kinases (1).

In the presence of NTN1, UNC5B dimerizes and its intracellular domain adopts a "closed" conformation, in which the ZU5 and the death domain interact. Death-associated protein kinase 1 (DAPK) interacts with this "closed" domain but stays in an

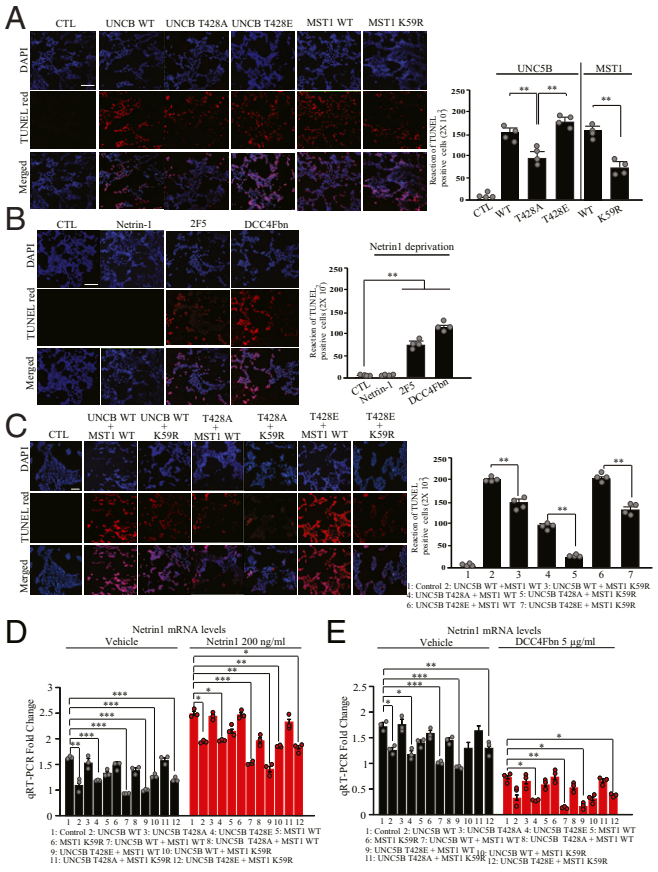

Fig. 4. Phosphorylation of UNC5B by MST1 mediates its proapoptotic activity. Quantification of the cellular apoptosis assays. (*A*) HEK293 cells were transfected with various plasmids (UNC5B WT, UNC5B T428A, UNC5B T428E, MST1 WT, and MST1 K59R) or their combinations (*B*), and cell apoptosis was analyzed via TUNEL staining deprivation of NTN1 from the medium via 2F5 anti-netrin monoclonal antibody or DCC-4Fbn for 24 h increased TUNEL-positive cells. (*C*) TUNEL-positive cells were found in cells cotransfected with MST1/UNC5B, and blockade of UNC5B phosphorylation by Mst1 reduced apoptosis. The bar graph in *A* shows the quantified TUNEL-positive cells; $n = 4$ each group. (Scale bar: 100 μm.) (*D* and *E*) Quantitative RT-PCR analysis of NTN1 mRNA levels in HEK293 cells stimulated with NTN1 (*D*) from HEK293 cells treated by DCC-4Fbn (*E*). CTL, control. Error bars represent the mean ± SEM. Statistical significance was determined using a two-way ANOVA followed by post hoc Bonferroni test for multiple group comparison. $^{*}P < 0.05$; $^{**}< 0.01$; $^{***}P < 0.001$.

inactive state via its autophosphorylation. In the absence of ligand, UNC5B is monomeric, its intracellular domain is cleaved, and this event triggers a conformational change ("open" confirmation that triggers DAPK activation and a proapoptotic signaling) (41). We have previously reported that NTN1 triggers UNC5B and PIKE-L association, which leads to PI3K/Akt signaling activation, promoting neuronal survival (20). In addition, we show that Akt directly phosphorylates MST1 T387 and inhibits its apoptotic activation (7). Conceivably, NTN1 deficiency elicits DAPK activation, which might elicit capsase-3 activation that cleaves MST1, leading to its autophosphorylation of T183 and full activation. Subsequently, p-MST1 phosphorylates UNC5B T428 and promotes its apoptotic cleavage by active caspase-3. Since MST1 and caspase-3 also mutually regulate each other's apoptotic activities (37), antagonizing MST1 phosphorylation and apoptotic activation via inactive UNC5B results in inhibition of MST1/LATS/YAP pathway and blockade of caspase-3 activation. Then, elevated total YAP promotes dopaminergic neuronal survival (Fig. 7*F*).

MST1/2 is activated by hydrogen peroxide and involved in cellular oxidative stress responses (4, 42). On the other hand, YAP physically interacts with FOXO1 and activates FOXO1-mediated transcription of catalase and MnSOD genes and subsequently reduces oxidative stress and ischemia/reperfusion-induced injury in the heart (30), implicating a physiological role of YAP in reactive oxygen species scavenging. Noticeably, MST1 is activated and implicated in neurodegenerative prion disease (43). YAP has also been implicated in neurodegenerative diseases, for instance, Huntington's disease. In transcriptional repression-induced atypical death of neurons, YAP's full length is reduced, promoting apoptosis. The dominant negative C terminus-truncated YAPΔCs markedly attenuate Htt-induced neuronal death in primary neuron and *Drosophila melanogaster* models (44). YAP and TAZ are transcriptional coactivators. When translocated into the nucleus, they regulate gene expression through interaction with TEAD1 to TEAD4, which are sequence-specific transcription factors that mediate the main transcriptional output of the Hippo pathway in mammalian cells (45). The major physiological functions of YAP and TAZ are to promote cell survival and proliferation (46). Our findings that NTN1 escalates YAP levels via inhibiting conventional Hippo/MST1 pathway and promotes cell survival are in alignment with the well-defined prosurvival functions of YAP. NTN1 is a laminin-related family member of secreted proteins. Netrins bind to numerous receptors including integrins (47). Interestingly, it has been reported that the extracellular matrix protein laminin-511 (LM511) promotes the survival and differentiation of dopaminergic neurons. LM511 binds to integrin α3β1 and activates the transcriptional cofactor YAP (48). Moreover, YAP prevents optic nerve injury-induced retinal apoptosis (49). These previous findings are consistent with our observations. For instance, we show that, when Mst1 is depleted by its Cre virus or blocked by overexpressing KD K59R mutant, YAP levels were greatly elevated even in the absence of NTN1, due to DCC-4Fbn treatment. As a result, caspase-3 activation is greatly inhibited, and dopaminergic neuronal loss is decreased (Fig. 6 and *SI Appendix*, Fig. S7). Moreover, we made a similar observations with UNC5B T428A mutant, which is unphosphorylated by MST1. Overexpression of T428A strongly suppressed NTN1 deprivation-induced MST1 apoptotic activation, leading to repression of p-LATS/p-YAP pathway, which culminates in repression of caspase-3 activation and mitigation of dopaminergic apoptosis (Fig. 5 and *SI Appendix*, Fig. S5). Blockade of UNC5B T428 phosphorylation by MST1 not only inhibits UNC5B apoptotic cleavage and reduces its proapoptotic activity but also attenuates MST1 apoptotic activation. Therefore, these findings support that UNC5B and MST1 mutually modulate each other's apoptotic functions via physical interaction and phosphorylation, and NTN1 regulates Hippo/MST1 signaling via its receptor UNC5B.

Methods

Mice and Cell Lines. The UNC5B f/f (8 wk old; a gift from Dean Y. Li, University of Utah, Salt Lake City, UT), MST1/2 f/f mice (tk3F/FStk4F/F mice [JAX stock #017635] were purchased from The Jackson Laboratory) or NTN1 f/f mice received 2 μL of the phosphate-buffered Cre recombinant lentivirus (1×10^8 plaque-forming units per mouse) by stereotaxic injection. Human embryonic kidney HEK293 cells were maintained in Dulbecco's modified Eagle's medium (DMEM) with 10% (vol/vol) fetal bovine serum (FBS) and 1× pen/strep/glutamine at 37 °C in a 5% (vol/vol) CO_2 atmosphere in a humidified incubator. SH-SY5Y cells were cultured in DMEM/F12 added to 10% FBS and penicillin (100 units/mL)–streptomycin (100 μg/mL) (all from HyClone). Cells were incubated at 37 °C in a humidified atmosphere of 5% CO_2. Animal care and handling was performed according to NIH animal care guidelines and Emory Medical School guidelines. The protocol was reviewed and approved by the Emory Institutional Animal Care and Use Committee.

Healthy Control and PD Postmortem Brain Samples. Postmortem brain samples were dissected from frozen brains of PD patients and age-matched

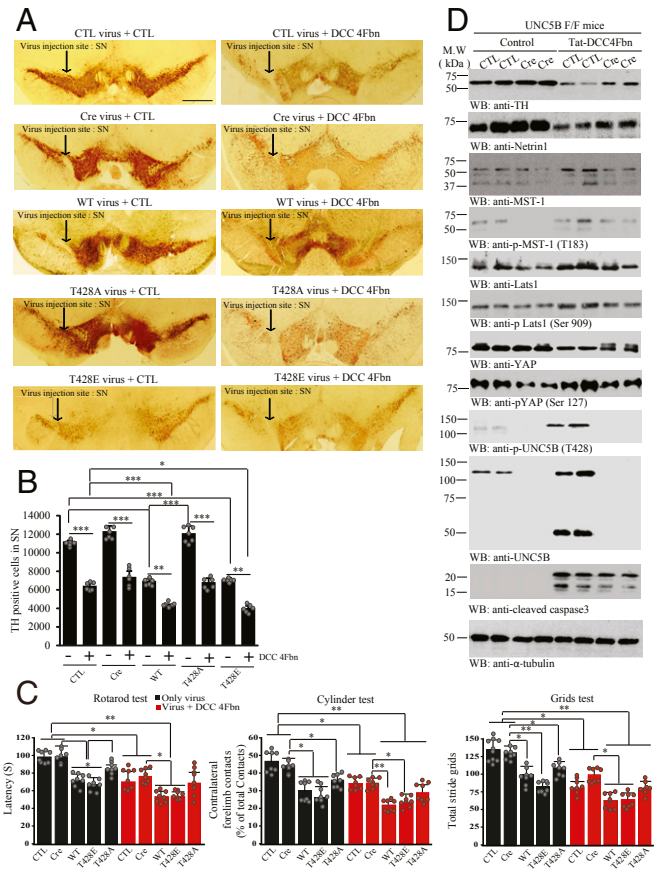

Fig. 5. UNC5B phosphorylation by MST1 is required for dopaminergic neuronal loss and motor dysfunctions. (*A*) IHC staining of TH in the SN of UNC5B f/f mice. Control virus, Cre virus, or UNC5B WT, UNC5B T428A, or UNC5B T428E virus was injected into the SN of UNC5B f/f mice, followed by treatment with Tat-DCC 4Fbn or vehicle control (i.p.). TH IHC was conducted on the brain sections of SN regions from UNC5B f/f mice. (Scale bar: 2,000 μm.) (*B*) Quantification of TH-positive cells in the SN. The graph is the stereological counted TH-positive cells; $n = 6$ each group. (*C*) Motor behavioral assays. Unphosphorylated UNC5B T428A protected dopaminergic neurons from DCC-4Fbn-induced cell loss as compared to UNC5B WT or T428E; $n = 8$ per group. Error bars represent the mean ± SEM. Statistical significance was determined using a two-way ANOVA followed by post hoc Bonferroni test for multiple group comparison. $*P < 0.05$; $**< 0.01$; $***P < 0.001$. (*D*) Deletion of UNC5B protects DCC-4Fbn-triggered dopaminergic neuronal loss in the SN of UNC5B f/f mice. Immunoblot of TH, NTN1, MST1, p-MST1 (T183), LATS1, p-LATS1 (Ser909), YAP, p-YAP (Ser127), UNC5B, p-UNC5B (T428), and cleaved caspase-3 levels in control (CTL) or Cre virus-injected UNC5B f/f brain (SN) lysate samples. Three independent experiments were conducted in all of the assays.

nondemented controls (55 y to 72 y old) from the Emory Alzheimer's Disease Research Center (ADRC). The study was approved by the Biospecimen Committee (The Goizueta ADRC, Emory University). PD was diagnosed according to the criteria of the Consortium to Establish a Registry for PD and the National Institute on Aging. Informed consent was obtained from all cases.

Transfecting Plasmid DNA into HEK 293 and SH-SY5Y Cells. HEK 293 and SH-SY5Y cells were transfected with plasmids encoding GFP-UNC5B and MST1 WT or GFP-UNC5B T428A, GFP-UNC5B T428E, and GFP-MST1 K59R using Lipofectamine 3000 (Thermo Fisher Scientific).

TUNEL Assay. At 12 wk after Tat-DCC-4Fbn i.p. injection, the mouse brains were fixed in 4% formaldehyde, permeabilized, and immune-stained with anti-TH antibody. The dopaminergic neuronal death induced by NTN1 depletion was detected with an in situ cell death detection kit (Roche, Cat# 11684795910). The apoptotic index was expressed as a percentage of TUNEL-positive neurons out of the total number of TH-positive neurons. Results presented for DNA fragmentation experiments are an average of three experiments conducted independently.

Cell Viability. Cell viability was measured calorimetrically using the Cell-Titer Blue (CTB, Promega) fluorescence-based assay. Cells were plated at a density of 1,000 cells per well in 96-well plates (BD Biosciences). Control vector, UNC5B WT, UNC5B T428A, UNC5B T428E, MST1 WT, and MST1 K59R plasmids were transfected with Lipofectamine 3000 (Thermo Fisher Scientific) to each well, and then incubated for an additional 2 d. After incubation, 30 μL of CTB reagent was added to each well and incubated at 37 °C and 5% CO_2 for 2.5 h to 5 h. Fluorescence of the resorufin product was measured on a FluoDia T70 fluorescence plate reader (Photon Technology International). Wells that included vehicle but not protein served as the negative control (0% toxic), and wells containing 10% dimethyl sulfoxide were the positive control (100% toxic). Results presented for viability experiments are an average of three experiments conducted independently on different days. Error bars represent the SEM.

Autoradiography. Purified GST-tagged UNC5H2 (413 to 945) or GST-tagged MST1 (1 to 326) proteins were incubated with control GST, MST1 T183A, or UNC5B T428A recombinant proteins with or without cross-tides in 20 μL of kinase reaction buffer (20 mM Tris, pH 7.5, with 10 mM $MgCl_2$) containing 25 μM ATP and 2.5 μCi of [γ-^{32}P]ATP for 30 min at 30 °C. Reactions were terminated by adding 7 μL of Laemmli's sample buffer. A portion of the sample (15 μL) was separated on sodium dodecyl sulfate polyacrylamide gel electrophoresis (SDS/PAGE) and autoradiographed, analyzed by a PhosphorImage analyzer, or subjected to liquid scintillation assay.

Immunoblotting. SH-SY5Y cells, HEK 293 cells or mouse brain were lysed in lysis buffer (50 mM Tris, pH 7.4, 40 mM NaCl, 1 mM ethylenediaminetetraacetic acid [EDTA], 0.5% Triton X-100, 1.5 mM Na_3VO_4, 50 mM NaF, 10 mM sodium pyrophosphate, and 10 mM sodium β-glycerophosphate, supplemented with a mixture of protease inhibitors), and centrifuged for 20 min at 4 °C 15,000 rpm for cell lysate or ultracentrifuged for 20 min at 4 °C 100,000 rpm for mouse brain tissues. The supernatant fraction was boiled in 1× SDS loading buffer. After SDS/PAGE, the samples were transferred to a nitrocellulose membrane. Primary antibodies to the following targets were used: HA (Cell signaling, Cat#2362), GST (Amersham, Cat#27-4577-01), Flag (Sigma, Cat#F3165), p-CEBPβ (Abcam, Cat#ab52194), alpha-synuclein pS129 (LS bio, Cat# LS-C380861-1), TH (Santa Cruz, Cat#SC-25269; Abcam, Cat# ab112), pMST1-T183 (Abcam, Cat# ab79199), MST1 (Cell signaling, Cat# 3682), YAP (Cell signaling, Cat#4912), pYAP–S129(Cell signaling, Cat#4911), UNC5B (R&D, Cat# MAB1006), pUNC5B-T428 (K.Y.'s Lab Cat# N/A), LATS1 (Abcam, Cat#ab70561), pLATS1-S909 (Cell signaling, Cat#9157), cleaved caspase-3 (Cell signaling Cat# 9661), NTN1 (Santa Cruz, Cat#SC-20786 and Abcam, Cat#Ab126729), AKT (Cell signaling, Cat#9272), pAKT-S473 (Cell signaling, Cat#3787), and LaminB1 (Santa Cruz, Cat#SC-377000).

CO-IP. The mouse brain tissue samples or transfected HEK 293 cells were lysed in lysis buffer (50 mM Tris, pH 7.4, 40 mM NaCl, 1 mM EDTA, 0.5% Triton X-100, 1.5 mM Na3VO4, 50 mM NaF, 10 mM sodium pyrophosphate, and 10 mM sodium β-glycerophosphate, supplemented with a mixture of protease inhibitors) and centrifuged for 15 min at 16,000 × *g*. The supernatant was incubated with anti-UNC5B or anti-MST1 antibodies and Protein A/G–agarose overnight at 4 °C. After extensive washing with lysis buffer, the bound proteins were eluted from the beads by boiling in Laemmli sample buffer and were subjected to Western blot analyses.

Immunofluorescence Staining. SH-SY5Y cells, mice, and human brain tissues were fixed 4% paraformaldehyde. The mouse brain tissues were fixed with 4% paraformaldehyde/30% sucrose (brain:SN) in PBS followed by permeabilization with PBS-T (50 mM Tris·HCl, 150 mM NaCl, 3% bovine serum albumin [BSA], 0.1% Triton-X100, pH7.4) solution. For the analysis of pathological changes for PD, the sections or slides from the fixed and sliced samples were incubated with the primary antibodies of TH (Santa Cruz, Cat#SC-25269; Abcam, Cat# ab112), pMST1-T183 (Abcam, Cat# ab79199), MST1 (Cell signaling, Cat# 3682), UNC5B (R&D, Cat# MAB1006), or pUNC5B-T428 (K.Y.'s Lab Cat# N/A). Then, the sections or slides were incubated with the fluoroconjugated secondary antibody for 1 h at room temperature, after washing three times in PBS. After DAPI staining for 5 min, the slides were washed three times in PBS and covered with a glass using mounting solution.

Perfusion and Tissue Processing for Immunofluorescence. Mice were anesthetized with an overdose of sodium pentobarbital (90 mg/kg, i.p.) and

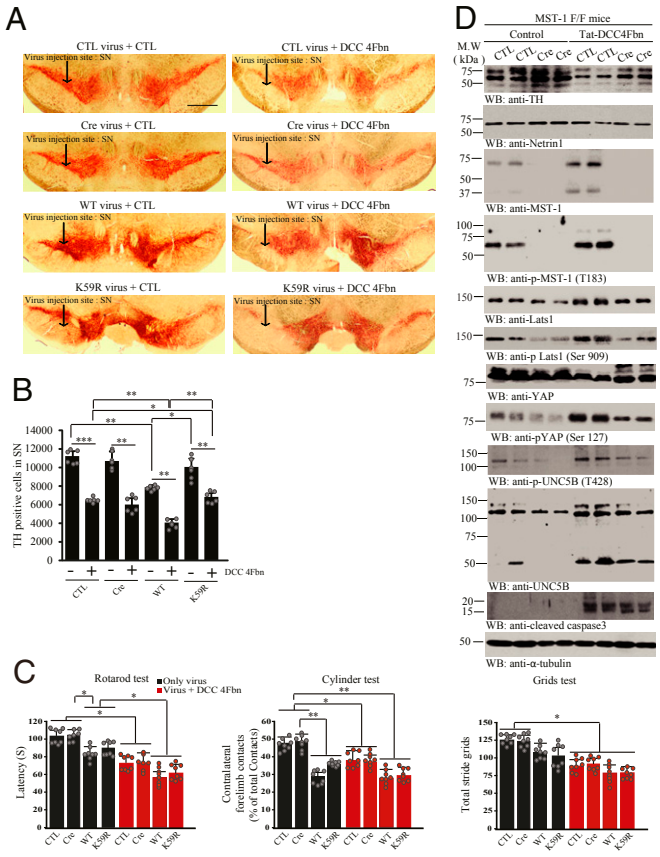

Fig. 6. MST1 kinase activity is required for DCC-4Fbn-induced dopaminergic neuronal loss and motor dysfunctions in MST1 f/f mice. (*A*) IHC staining of TH in the SN of MST1 f/f mice. Control, Cre, MST1 WT, or MST1 K59R virus was injected into the SN regions of MST1 f/f mice, followed by treatment with Tat-DCC-4Fbn (i.p.). Dopaminergic neuronal loss in the brain (SN) was analyzed by TH IHC analysis. (Scale bar: 2,000 μm.) (*B*) Quantification of TH-positive neurons. The bar graph is stereological counted TH-positive cells quantified result; $n = 6$ independent experiments. (*C*) Motor behavioral assays; $n = 8$ each group. Error bars represent the mean ± SEM. Statistical significance was determined using a two-way ANOVA followed by post hoc Bonferroni test for multiple group comparison. $*P < 0.05$; $**< 0.01$; $***P < 0.001$. (*D*) Deletion of MST1 decreases DCC-4Fbn–stimulated TH loss. Immunoblot analysis of TH, NTN1, MST1, p-MST1(T183), LATS1, p-LATS1(Ser909), YAP, p-YAP(Ser127), UNC5B, p-UNC5B(T428), and cleaved caspase-3 levels in control (CTL) or Cre virus-injected MST1 f/f brain (SN) lysate samples. Three independent experiments were conducted.

perfused intracardially with PBS followed by 4% paraformaldehyde in a 0.1 M sodium phosphate buffer, pH 7.4. Brains were removed, post-fixed overnight, and stored in sodium phosphate buffer containing 30% sucrose at 4 °C. Serial frozen sections of 30 μm (mouse brain samples) thickness were made using a cryostat. Six sets of sections were collected in a cryoprotectant solution (0.1 M phosphate buffer, pH 7.4, 20% glycerol, and 2% dimethyl sulfoxide) and stored at −20 °C until immunofluorescence processing.

IHC. Mouse brain sections sliced by cryotome or paraffin-embedded human brain sections were treated with 0.3% H_2O_2 for 10 min. Sections were washed three times in PBS and blocked in 1% BSA, 0.3% Triton X-100, for 30 min, followed by overnight incubation with TH antibody (1: 1000) or p-UNC5B T428 antibody (1: 300) at 4 °C. The signal was developed using Histostain-SP kit (Invitrogen).

Stereological Cell Quantification. Unbiased stereological cell counting was performed using the Stereo Investigator software (MBF Bioscience). All SN sections of 30 μm at every sixth section were stained with TH antibody. They were analyzed under the randomly placed counting frames (50 × 50 μm) on a counting grid (120 × 120 μm). Optical dissector of 22 μm with 2-μm upper and lower guard zones was used. The boundaries of SN were outlined under magnification of the 5× objective lens, and cells were counted with the 40× objective lens using an Olympus BX53 microscope. The total number of neurons in the SN was estimated using the optical fractionator method. TH-positive axon terminal in striatum was estimated using fluorescence intensity by Image J software. For quantification of positive cells, stained color was selected and set the proper threshold for the binarization of the selected color image. The total number of immune-reactive neurons was analyzed using the same threshold (Image J). The conditions of the analysis were blinded to the investigator.

Stereotaxic Injection. Two- or three-month-old mice of each group (UNC5B WT, UNC5B T428A, UNC5B T428E, MST1 WT, MST1 K59R, and Cre virus) were anesthetized with isoflurane. Meloxicam (5 mg/kg) was injected subcutaneously for analgesics (Loxicom). Unilateral stereotaxic injection of virus was performed at coordinates corresponding to the SN: anteroposterior: ±3.1 mm, mediolateral: ±1.2 mm from Bregma, and dorsoventral: −4.3 mm from dura surface. Each site received 2 μL of viruses: AAV6-Cre (1×10^{12}), Lenti-Sh

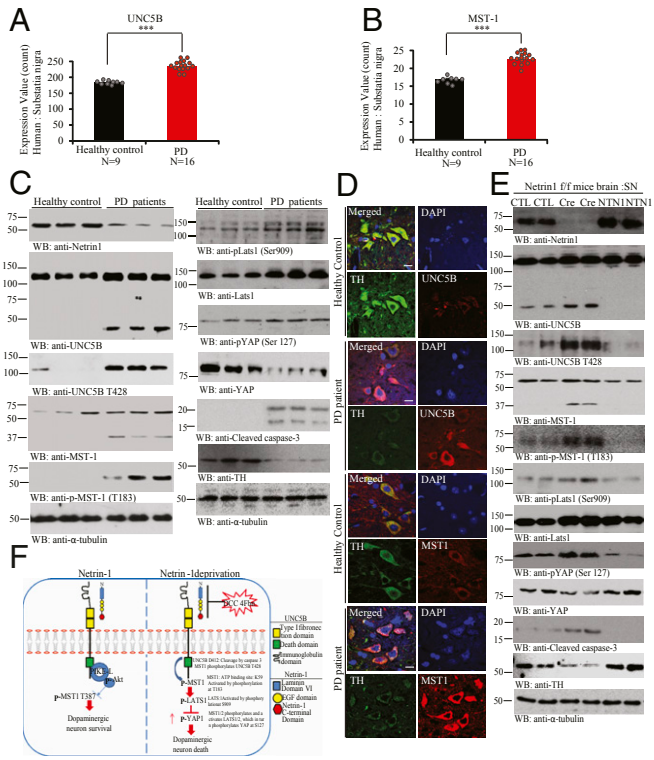

Fig. 7. UNC5B and MST1 phosphorylation and activation in PD patient's brains. (*A* and *B*) Quantification of UNC5B and MST1 expression levels in healthy control or PD patient brains. (*A*) UNC5B and (*B*) MST1 genes expression profiling by arrays of PD SN from datasets GDS2821. (Unpaired *t* test, $***P < 0.0005$, means + SD are shown.) (*C*) NTN1 reduction in PD brains is associated with Mst1 activation and phosphorylation of UNC5B and TH loss. Immunoblot of NTN1, UNC5B, p-UNC5B (T428), MST1, p-MST1 (T183), p-LATS1 (Ser909), LATS1, p-YAP (Ser127), YAP, TH, and cleaved caspase-3 levels in age-matched healthy control vs. PD patients brain tissue samples. Three independent studies were conducted in all of the experiments. (*D*) IF costaining reflects the inverse correlation of MST1/TH and UNC5B/TH in the human brain sections. The SN regions from healthy control or PD patient brain sections were costained with indicated antibodies. TH/UNC5B or TH/MST1 coimmunostaining representative images were conducted in age-matched healthy control vs. PD patient's brain paraffin slides. Three independent blinder tests were conducted in all of experiments. (Scale bar: 50 μm.) (*E*) NTN1 depletion from NTN1 f/f mice elicits MST1 phosphorylation of UNC5B T428 and TH loss, which is blocked by NTN1 overexpression. Representative immunoblotting images of SN tissues from AAV6-GFP (control virus), AAV6-GFP Cre, or hNTN1 virus-injected NTN1 f/f mice brain. Three independent studies were conducted in all of the experiments. (*F*) The schematic model of NTN1 deprivation-elicited Hippo/MST1 signaling pathway via UNC5B receptor. CTL, control.

UNC-5B WT (1×10^{10}), AAV6-GFP-UNC5B T428A (1×10^{12}), AAV6-GFP-UNC5B T428E (1×10^{12}), Lenti-Sh Mst1 WT (1×10^{10}), and AAV6-GFP-Mst1 K59R (1×10^{10}) at a rate of 0.25 μL/min, using a 10-μL Hamilton syringe. The needle was kept in place for 5 min after the injection was completed, and then gently removed. Mice were placed on a heating pad until they recovered from the anesthesia.

Generation of Antibodies Specific p-UNC5B T428 Antibody. The rabbits were immunized with the peptide Ac-HPVNFKpTARPSNPQ-OH, which included the 14 amino acids in UNC5B that precede phosphorylate site at T428. The rabbits received booster injections four times with the immunizing peptide, with 3-wk intervals between injections. The antiserum was affinity purified by chromatography with the immunizing peptide and then was absorbed to a spanning peptide spanning the T428 phosphorylate site (Ac-HPVNFKTARPSNPQ-amide). The titers against the immunizing peptide were determined by enzyme-linked immunosorbent assay. The maximal dilution giving a positive response with chromogenic substrate for horseradish peroxidase was 1:30,000. The immunoactivity of the antiserum was further confirmed by Western blotting and IHC.

Behavioral Tests. Loss of motor function was tested at 12 weeks later from 7 different virus (Cre, UNC5B WT, UNC5B T428A, UNC5B T428E, MST1 WT, and MST1 K59R) injected mice with Tat-DCC-4Fbn i.p. injection. Behavioral test included the rotarod test, cylinder test, and grid test. Rotarod test: Mice were trained for 3 d using the Rotarod (San Diego Instruments) at a slow rotational speed (5 rpm) for a maximum of 10 min. The rotational speed and latency to fall from the accelerating Rotarod were recorded, after three test trials on the test day. The rotational speed of Rotarod was modulated from 0 rpm to a maximum 40 rpm. It was gradually increased during the trial at a rate of 0.1 rpm/s. Cylinder test: Mice were placed individually into a glass cylinder (12 cm diameter × 22 cm height) and recorded by video camera. The recorded files were analyzed by a blinded observer. Between 20 and 30 wall touches per animal (contacts with fully extended digits executed with the forelimb ipsilateral and contralateral to the lesion) were counted. Grid performance test: The mice were placed on a horizontal grid. The grid was inverted, so the mice were hanging upside down by their paws. Animals were videotaped for up to 60 s, and then a 10-s segment was scored for forepaw step distance as defined by the number of grids traversed with each step.

Quantification and Statistical Analysis. Statistical analysis of results was performed using GraphPad (Prism). All data were tested for normal distribution in order to analyze results accordingly using parametric or nonparametric tests. To compare results between two groups, Student's unpaired *t* test was used. When more than two groups were compared, one-way ANOVA followed by Tukey post hoc test was applied. For repeated measures, a Repeated-measures ANOVA or two-way ANOVA test was performed followed by Bonferroni post hoc multiple comparison analysis. A value of $P < 0.05$ was considered to be statistically significant. Effect size of samples was determined by Power analysis (Biostat).

Data and Materials Availability. UNC5B, MST1, and NTN1 gene expression profiling by array of PD SN was obtained from GDS 2821 series available on GEO database. All other data are available in the main text or *SI Appendix*.

ACKNOWLEDGMENTS. The authors are grateful for Dr. Patrick Mehlen from University of Lyon for the precious reagents including anti-Netrin-1 and 4Fbn recombinant proteins. This work was supported by grants from the NIH (Grants RF1 and AG051538) to K.Y. We thank ADRC at Emory University for human PD patients and healthy control samples. This study was supported, in part, by the Rodent Behavioral Core, which is subsidized by the Emory University School of Medicine and is one of the Emory Integrated Core Facilities. Additional support was provided by the Viral Vector Core of the Emory Neuroscience National Institute of Neurological Disorders and Stroke (NINDS) Core Facilities (P30N program S055077). Further support was provided by the Georgia Clinical & Translational Science Alliance of the NIH under Award UL1TR002378.

1. Z. Meng, T. Moroishi, K. L. Guan, Mechanisms of Hippo pathway regulation. *Genes Dev.* **30**, 1–17 (2016).
2. F. X. Yu *et al*., Regulation of the Hippo-YAP pathway by G-protein-coupled receptor signaling. *Cell* **150**, 780–791 (2012).
3. Y. Zheng, D. Pan, The Hippo signaling pathway in development and disease. *Dev. Cell* **50**, 264–282 (2019).
4. M. K. Lehtinen *et al*., A conserved MST-FOXO signaling pathway mediates oxidative-stress responses and extends life span. *Cell* **125**, 987–1001 (2006).
5. A. Ardestani *et al*., MST1 is a key regulator of beta cell apoptosis and dysfunction in diabetes. *Nat. Med.* **20**, 385–397 (2014).
6. P. Zhang *et al*., Exploration of MST1-mediated secondary brain injury induced by intracerebral hemorrhage in rats via Hippo signaling pathway. *Transl. Stroke Res.* **10**, 729–743 (2019).
7. S. W. Jang, S. J. Yang, S. Srinivasan, K. Ye, Akt phosphorylates MstI and prevents its proteolytic activation, blocking FOXO3 phosphorylation and nuclear translocation. *J. Biol. Chem.* **282**, 30836–30844 (2007).
8. T. E. Kennedy, M. Tessier-Lavigne, Guidance and induction of branch formation in developing axons by target-derived diffusible factors. *Curr. Opin. Neurobiol.* **5**, 83–90 (1995).
9. P. B. Osborne, G. M. Halliday, H. M. Cooper, J. R. Keast, Localization of immunoreactivity for deleted in colorectal cancer (DCC), the receptor for the guidance factor netrin-1, in ventral tier dopamine projection pathways in adult rodents. *Neuroscience* **131**, 671–681 (2005).
10. L. Lin, O. Isacson, Axonal growth regulation of fetal and embryonic stem cell-derived dopaminergic neurons by Netrin-1 and Slits. *Stem Cells* **24**, 2504–2513 (2006).
11. J. Li *et al*., Evidence for topographic guidance of dopaminergic axons by differential Netrin-1 expression in the striatum. *Mol. Cell. Neurosci.* **61**, 85–96 (2014).
12. P. Mehlen *et al*., The DCC gene product induces apoptosis by a mechanism requiring receptor proteolysis. *Nature* **395**, 801–804 (1998).
13. C. Forcet *et al*., The dependence receptor DCC (deleted in colorectal cancer) defines an alternative mechanism for caspase activation. *Proc. Natl. Acad. Sci. U.S.A.* **98**, 3416–3421 (2001).
14. F. Llambi, F. Causeret, E. Bloch-Gallego, P. Mehlen, Netrin-1 acts as a survival factor via its receptors UNC5H and DCC. *EMBO J.* **20**, 2715–2722 (2001).
15. C. Tanikawa, K. Matsuda, S. Fukuda, Y. Nakamura, H. Arakawa, p53RDL1 regulates p53-dependent apoptosis. *Nat. Cell Biol.* **5**, 216–223 (2003).
16. S. Reyes *et al*., Trophic factors differentiate dopamine neurons vulnerable to Parkinson's disease. *Neurobiol. Aging* **34**, 873–886 (2013).
17. L. Lin, T. G. Lesnick, D. M. Maraganore, O. Isacson, Axon guidance and synaptic maintenance: Preclinical markers for neurodegenerative disease and therapeutics. *Trends Neurosci.* **32**, 142–149 (2009).
18. T. G. Lesnick *et al*., Beyond Parkinson disease: Amyotrophic lateral sclerosis and the axon guidance pathway. *PLoS One* **3**, e1449 (2008).
19. K. Ye, S. H. Snyder, PIKE GTPase: A novel mediator of phosphoinositide signaling. *J. Cell Sci.* **117**, 155–161 (2004).
20. X. Tang *et al*., Netrin-1 mediates neuronal survival through PIKE-L interaction with the dependence receptor UNC5B. *Nat. Cell Biol.* **10**, 698–706 (2008).
21. P. Mehlen, F. Llambi, Role of netrin-1 and netrin-1 dependence receptors in colorectal cancers. *Br. J. Cancer* **93**, 1–6 (2005).
22. Q. Qi, D. Y. Li, H. R. Luo, K. L. Guan, K. Ye, Netrin-1 exerts oncogenic activities through enhancing Yes-associated protein stability. *Proc. Natl. Acad. Sci. U.S.A.* **112**, 7255–7260 (2015).
23. W. L. Cheung *et al*., Apoptotic phosphorylation of histone H2B is mediated by mammalian sterile twenty kinase. *Cell* **113**, 507–517 (2003).
24. A. Paradisi *et al*., Netrin-1 up-regulation in inflammatory bowel diseases is required for colorectal cancer progression. *Proc. Natl. Acad. Sci. U.S.A.* **106**, 17146–17151 (2009).
25. H. Chen, Q. Chen, Q. Luo, Expression of netrin-1 by hypoxia contributes to the invasion and migration of prostate carcinoma cells by regulating YAP activity. *Exp. Cell Res.* **349**, 302–309 (2016).
26. K. Yin *et al*., Netrin-1 promotes metastasis of gastric cancer by regulating YAP activity. *Biochem. Biophys. Res. Commun.* **496**, 76–82 (2018).
27. H. Arakawa, Netrin-1 and its receptors in tumorigenesis. *Nat. Rev. Cancer* **4**, 978–987 (2004).
28. L. Xiao *et al*., The c-Abl-MST1 signaling pathway mediates oxidative stress-induced neuronal cell death. *J. Neurosci.* **31**, 9611–9619 (2011).
29. Z. Yuan *et al*., Regulation of neuronal cell death by MST1-FOXO1 signaling. *J. Biol. Chem.* **284**, 11285–11292 (2009).
30. S. Zhao *et al*., Hippo/MST1 signaling mediates microglial activation following acute cerebral ischemia-reperfusion injury. *Brain Behav. Immun.* **55**, 236–248 (2016).
31. M. Khan, B. P. F. Rutten, M. O. Kim, MST1 regulates neuronal cell death via JNK/Casp3 signaling pathway in HFD mouse brain and HT22 cells. *Int. J. Mol. Sci.* **20**, E2504 (2019).
32. H. Tian, K. Wang, M. Jin, J. Li, and Y. Yu, Proinflammation effect of Mst1 promotes BV-2 cell death via augmenting Drp1-mediated mitochondrial fragmentation and activating the JNK pathway. *J. Cell Physiol.* **235**, 1504–1514 (2019).
33. C. L. Creasy, D. M. Ambrose, J. Chernoff, The Ste20-like protein kinase, Mst1, dimerizes and contains an inhibitory domain. *J. Biol. Chem.* **271**, 21049–21053 (1996).
34. J. A. Galan, J. Avruch, MST1/MST2 protein kinases: Regulation and physiologic roles. *Biochemistry* **55**, 5507–5519 (2016).
35. J. D. Graves, K. E. Draves, Y. Gotoh, E. G. Krebs, E. A. Clark, Both phosphorylation and caspase-mediated cleavage contribute to regulation of the Ste20-like protein kinase Mst1 during CD95/Fas-induced apoptosis. *J. Biol. Chem.* **276**, 14909–14915 (2001).
36. K. K. Lee, T. Ohyama, N. Yajima, S. Tsubuki, S. Yonehara, MST, a physiological caspase substrate, highly sensitizes apoptosis both upstream and downstream of caspase activation. *J. Biol. Chem.* **276**, 19276–19285 (2001).
37. H. Glantschnig, G. A. Rodan, A. A. Reszka, Mapping of MST1 kinase sites of phosphorylation. Activation and autophosphorylation. *J. Biol. Chem.* **277**, 42987–42996 (2002).

38. J. C. Boggiano, P. J. Vanderzalm, R. G. Fehon, Tao-1 phosphorylates Hippo/MST kinases to regulate the Hippo-Salvador-Warts tumor suppressor pathway. *Dev. Cell* **21**, 888–895 (2011).
39. C. L. Poon, J. I. Lin, X. Zhang, K. F. Harvey, The sterile 20-like kinase Tao-1 controls tissue growth by regulating the Salvador-Warts-Hippo pathway. *Dev. Cell* **21**, 896–906 (2011).
40. M. Praskova, A. Khoklatchev, S. Ortiz-Vega, J. Avruch, Regulation of the MST1 kinase by autophosphorylation, by the growth inhibitory proteins, RASSF1 and NORE1, and by Ras. *Biochem. J.* **381**, 453–462 (2004).
41. P. Mehlen, S. Tauszig-Delamasure, Dependence receptors and colorectal cancer. *Gut* **63**, 1821–1829 (2014).
42. J. Geng *et al*., Kinases Mst1 and Mst2 positively regulate phagocytic induction of reactive oxygen species and bactericidal activity. *Nat. Immunol.* **16**, 1142–1152 (2015).
43. R. H. Shott, A. Majer, K. L. Frost, S. A. Booth, L. M. Schang, Activation of pro-survival CaMK4β/CREB and pro-death MST1 signaling at early and late times during a mouse model of prion disease. *Virol. J.* **11**, 160 (2014).
44. M. Hoshino *et al*., Transcriptional repression induces a slowly progressive atypical neuronal death associated with changes of YAP isoforms and p73. *J. Cell Biol.* **172**, 589–604 (2006).
45. B. Zhao *et al*., TEAD mediates YAP-dependent gene induction and growth control. *Genes Dev.* **22**, 1962–1971 (2008).
46. J. Dong *et al*., Elucidation of a universal size-control mechanism in *Drosophila* and mammals. *Cell* **130**, 1120–1133 (2007).
47. F. Larrieu-Lahargue, K. R. Thomas, D. Y. Li, Netrin ligands and receptors: Lessons from neurons to the endothelium. *Trends Cardiovasc. Med.* **22**, 44–47 (2012).
48. D. Zhang *et al*., Niche-derived laminin-511 promotes midbrain dopaminergic neuron survival and differentiation through YAP. *Sci. Signal.* **10**, eaal4165 (2017).
49. J. X. Zhou *et al*., Low-intensity pulsed ultrasound protects retinal Ganglion cell from optic nerve injury induced apoptosis via yes associated protein. *Front. Cell. Neurosci.* **12**, 160 (2018).